ACS OMEGA

http://pubs.acs.org/journal/acsodf
Article

Adsorption Performance and Mechanism of Low Antimonate Concentrations in Water by Zirconium-Modified Biochar

Xueyi Shen, Siyi Ma, and Siqin Xu*

Cite This: https://doi.org/10.1021/acsomega.5c01523
Read Online

ABSTRACT: The widespread products using contained antimony and corresponding activities of Sb mining have led to elevated antimony concentrations in water. In order to effectively remove the excessive antimony in water, zirconium-modified peanut shell biochar (BC) was prepared. The effects of different environmental factors on antimony(V) adsorption and the recycling capacity, and practical application of the material were also studied, and its removal mechanism was revealed. The maximum adsorption capacity of antimony(V) by zirconium-modified BC reached 72.34 mg·g^{-1}. When coexisting ions were present, adsorptive inhibition of antimony(V) adsorption by zirconium-modified BC ranged from 0.74% to 21.68% apart from dihydrogen phosphate and arsenic(V), indicating selectivity of adsorption. Adsorptive isotherms analyses showed that the adsorption of antimony(V) by ZrBC was consistent with multilayer adsorption, and kinetic studies indicated that adsorptive procedures were predominantly chemisorptive. Zirconium-modified BC showed 100% removal rate after 4 reuse cycles and adsorption−desorption cycles, and the desorption amount was 6.16 mg·g^{-1}. The zirconium-modified BC adsorbed 6.97 mg·g^{-1} of antimony when treating real wastewater, which has potential for practical applications. Characterizations showed that the antimony(V) adsorptive mechanism in water mainly includes ligand exchange, complexation, electrostatic interaction, and hydrogen bonding. In summary, zirconium-modified BC can efficiently and stably remove Sb from the aqueous environment and can be a potentially viable option for antimony-containing wastewater treatment.

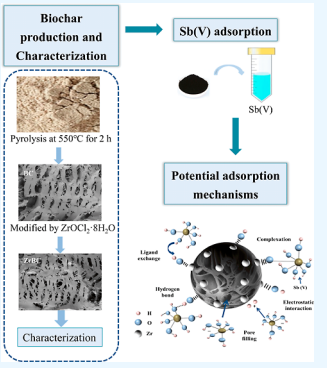

KEYWORDS: *modified biochar, zirconium, adsorption, low-concentration antimonate*

1. INTRODUCTION

Because of rapid industrialization and urbanization, antimony (Sb) concentration in our environment is increasing. Chronic intake of antimony-tainted food can cause a range of health problems, such as reproductive damage, developmental disorders, immune dysfunction, and neurological toxicity, which can cause serious threats to human well-being.[1] As a result, Sb is classified as priority pollutants by U.S. Environmental Protection Agency (USEPA) and Council of the European Union (EU).[2] Global Sb reserves exceed 1.8 million tons, with over 80% of output centered around Southwest China (such as Dushan and Dashan mines).[3] Massive Sb mine misuse and industrial development have led to the anthropogenic emission of significant quantities of Sb ions into their surroundings. Antimony concentrations in some polluted waters were high, from 100 to 7000 mg·L^{-1},[4] far exceeds Chinese emission limit (GB30770-2014, 0.3 mg·L^{-1}). Both antimony(III) and antimony(V) are the main Sb types found all over aqueous surroundings but Sb(V) has better solubility and migration rate.[5] Thus, studies on the effective Sb(V) removal in water are essential for protecting the water environment.

Based on current studies, membrane separation techniques,[6] flocculation/coagulation,[7] ion exchange,[8] adsorption,[9] and electrochemical treatments[10] have been used to remove Sb.[11] Of these, adsorptive approaches are one of the most widespread applications because of the numerous characteristics, such as large adsorption capacity, high cost-effectiveness, less secondary pollution to the environment, and flexible operation.[12] Zirconium exhibits high coordination ability and strong ionic affinity, particularly toward oxygen-containing functional groups. It is thermally stable, nontoxic, and remains stable across a wide pH range in aqueous solutions.[13] Based on these advantages, zirconium-based materials show significant potential in antimony adsorption. Research found that the zirconium metal-synthesized MOFs had maximum adsorption capacities of 136.97 mg·g^{-1} and 287.88 mg·g^{-1} for Sb(III) and Sb(V), respectively, and could reduce 100 μg·L^{-1} of Sb to about 2 μg·L^{-1} within 10 min.[14] However, zirconium is difficult to immobilize, separate, and recycle, limiting its practical application.[15] To overcome these drawbacks, some studies have considered loading zirconium on porous materials.[16] Biochar (BC) is an inexpensive and environ-

Received: February 18, 2025
Revised: June 19, 2025
Accepted: June 24, 2025

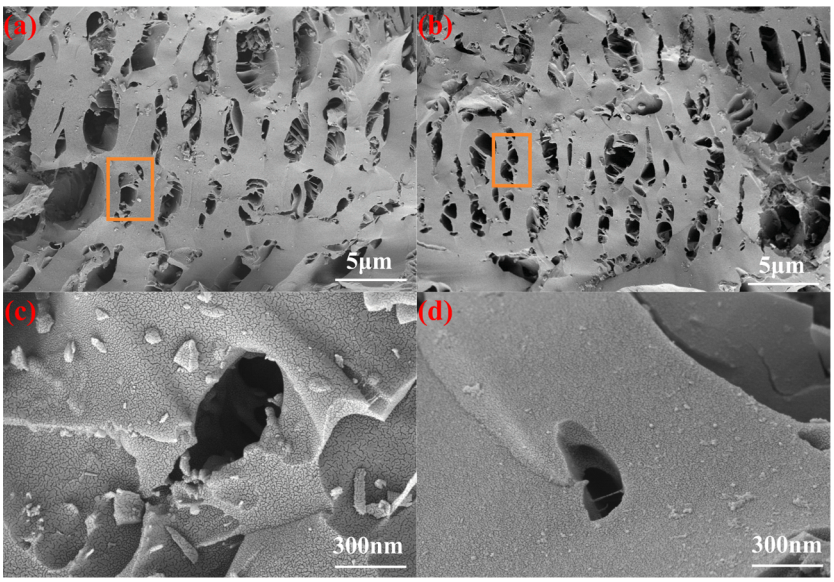

Figure 1. SEM images of BC and ZrBC. (a,c) BC. (b,d) ZrBC. Magnification of (a,b): 4 KX, magnification of (c,d): 60 KX.

mentally friendly porous adsorbent that can be used to load functional materials.[17] However, as a negatively charged surface, the primitive BC has poor adsorptive ability to anionic substances.[18] The adsorptive ability of BC to Sb in water can be significantly improved by appropriate modified treatment. In view of this, the research on the modification of BC has attracted much attention. BC can be modified in various ways, and the commonly used approaches are chemical modification, including acid modification, alkali modification, metal/metal oxide loading modification, and organic compound modification.[19,20] By loading metal/metal oxides, pore properties and oxygenated groups could be strengthened to promote cationic $\pi-\pi$ bonds, surface complexation, ion exchange, and electrostatic attraction of heavy metals with the BC. Introduction of iron-based materials, such as iron salts, iron (hydro)oxides, natural iron ores, is a simple and effective way to modify BC with metals.[21] The maximum adsorption capacity of Sb(III) by nano zerovalent iron-modified rice straw BC was 98.25 mg·g^{-1}.[22] However, iron ions may be released into processed wastewater, particularly under lower pH, and this may affect aquatic environment.[23] To address the issue of metal stability, researchers have begun to focus on more environmentally stable zirconium-based modified materials. Zirconium is stable in water and its modified materials have less zirconium leaching during adsorption.[24] It showed that zirconium-modified BC can work in removing some anionic pollution in water, like arsenic,[25] sulfate ions,[18] fluoride,[26] and Cr(VI).[27] Actual Sb pollution level in aquatic waters is usually low, for example, in the surface water of Weishan mine area, Banpo antimony mine area, and the rivers near Xunyang Hg−Sb mine in China, Sb concentrations were 1.20−1.72 mg·L^{-1}, 1.37 mg·L^{-1}, and 1.58 mg·L^{-1}, respectively. Despite some studies reporting excellent Sb removal efficiencies, effectively reducing Sb concentrations to less than 0.3 mg·L^{-1} at a reasonable cost remains a significant challenge.

In the research, peanut shell BC was produced and modified with zirconium oxychloride to obtain modified biochar (ZrBC), with 1 mg·L^{-1} Sb(V) selected as the experiment concentration. Isothermal, kinetic, thermodynamic, environmental impact factors, and practical application potentialcyclic were carried out. The materials were also characterized and analyzed. The primary goals were to investigate the effectiveness of removing low Sb(V) concentrations by modified BC in various adsorption setups, as well as to understand the possible adsorption processes and mechanisms.

2. RESULTS AND DISCUSSION

2.1. Characterization of Adsorbents. *2.1.1. SEM−EDS Analysis.* Scanning electron microscopy (SEM) scans for BC and ZrBC surface morphology are presented at Figure 1a−d. Figure 1a,b shows the morphology of BC and ZrBC at a magnification of 4 KX, and the morphology of BC and ZrBC at a magnification of 60 KX is shown in Figure 1c,d, respectively. As seen in Figure 1a, BC has porosity structures with coarse surfaces, favoring the provision of more active sites and at the same time providing space for zirconium loading. Comparing Figure 1b,d shows that the ZrBC surface was agglomerated with very fine particles, which may be zirconium oxide/hydroxide loaded. In addition, in the energy-dispersive X-ray spectroscopy (EDS) spectra (Figure S1a,b), it was observed that no Zr was found on the surface of BC, and Zr was seen on the surface of ZrBC with 15.43% (Table 1) atomic content, suggesting that Zr was loading successively on BC.

Table 1. Surface Atom Composition of BC and ZrBC

	surface atom composition (m %)		
materials	C	O	Zr
BC	92.67	7.33	0
ZrBC	76.93	7.64	15.43

2.1.2. BET Analysis. Adsorption−desorption curves for BC and ZrBC are given in Figures S1c,d, and Table S3 provides specific parameters. According to International Union of Pure and Applied Chemistry (IUPAC) classification, both BC and ZrBC were H4 hysteresis loop type IV curves, suggesting that adsorbents were mesoporous in structure. The hysteresis curve in BC was unclosed, possibly as a result of diffusive or chemotrap formed during the adsorptive process.[28] Compared with BC, the specific surface area and total pore volume of

https://doi.org/10.1021/acsomega.5c01523
ACS Omega XXXX, XXX, XXX−XXX

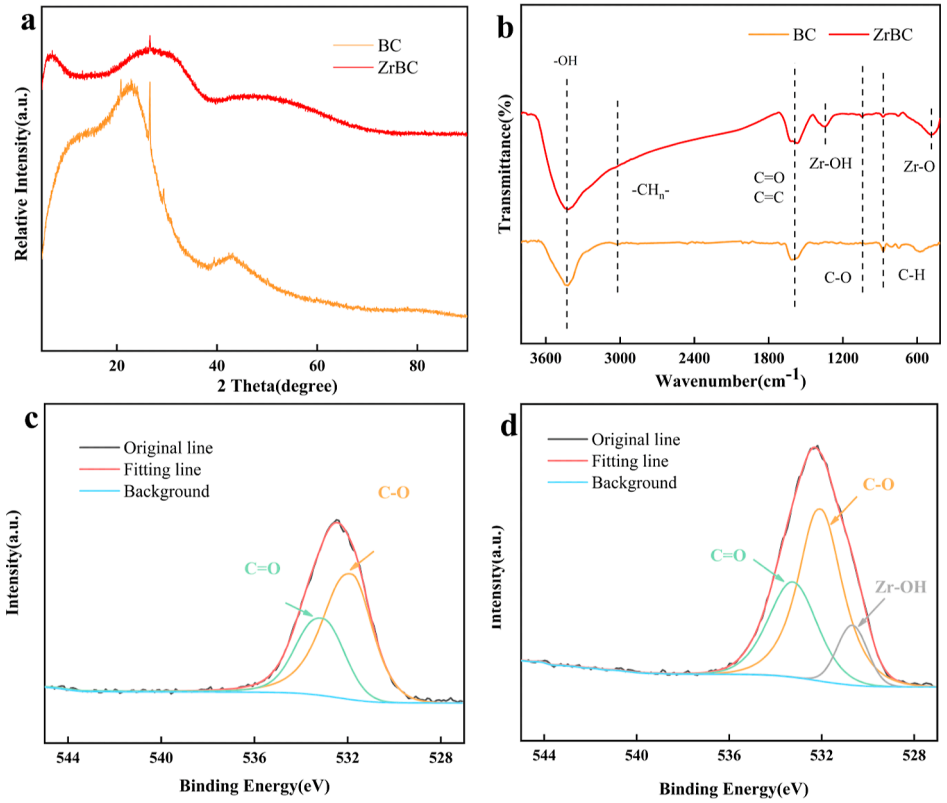

Figure 2. XRD, FT-IR, and XPS spectra for BC and ZrBC. (a) XRD. (b) FT-IR. (c), (d) XPS, O 1s spectra.

ZrBC increased by 96.62 $m^3 \cdot g^{-1}$ and 0.055 $cm^3 \cdot g^{-1}$, respectively, and the average pore size decreased by 4.37 nm. This indicated that it had a richer pore structure, providing additional adsorptive sites to Sb(V), in agreement with findings of SEM analyses.

2.1.3. XRD and FT-IR Analyses. BC and ZrBC crystal patterns were determined by X-ray diffraction (XRD) (Figure 2a). Broad diffraction peaks in Figure 2a confirm that BC and ZrBC are mainly present in the amorphous phase.[17] In addition, diffraction peaks at 28.27° and 50.83° were found in the XRD spectrograms of ZrBC, corresponding to ZrO_2 crystalline faces.[29] The analyses showed BC succeeded in achieving the loading of Zr.

Fourier transform infrared spectrometry (FT-IR) results are shown in Figure 2b. Absorptive peaks near 3422 and 580 cm^{-1} were attributed to stretching and bending vibrations of the hydroxyl group (−OH).[30] Band near 3011 cm^{-1} was consistent with aliphatic hydrocarbons ($-CH_n-$).[31] Absorptive peak near 1592 cm^{-1} stood for C═C and C═O.[32,33] Bands on 1045 and 872 cm^{-1} represented bending vibration of C−O[34] and stretching vibration for −CH−,[35] respectively. This was since this biomass was enriched with function groups, which were retained when it was charred. After modification, the other absorption peaks of ZrBC were found at 1349 and 493 cm^{-1}, respectively, resulting from the stretching vibrations of Zr−OH and Zr−O,[36,37] which suggested successful loading of Zr. These results confirmed that zirconium-modification enhanced function group abundance on BC.

2.1.4. XPS Analysis. X-ray photoelectron spectroscopy (XPS) results for BC and ZrBC were analyzed. The O 1s spectra are shown in Figure 2c,d and the full spectra in Figure S2. The C 1s, O 1s, and Zr 3d peaks for materials were distinctly marked following correction for reference binding energy for C 1s (284.80 eV). We evaluated O 1s spectra (Figure 2c,d). Table S7 provides specific elements of BC and ZrBC. O 1s spectral analyses showed that BC surface contained two main functional groups, C−O (62.89%) and C═O (37.11%), whereas ZrBC surface contained three main components, C−O (55.41%), C═O (32.36%), and Zr−OH (12.23%). In the full spectra of ZrBC, peaks corresponding to Zr 3d (Figure S2) can be identified, further verifying the success of Zr introduction at the BC surface.

2.2. Influences on Sb(V) Adsorption. *2.2.1. Impact of BC and ZrBC Dosage on Adsorption.* Figure S3a illustrates influence of BC and ZrBC dosage for Sb(V) adsorptive capacity. The adsorption capacity (q_e) and removal rate of Sb(V) by both adsorbents were affected by the dosage. Adsorption capacity was negatively correlated with the dosage due to unsaturated adsorptive sites in adsorptive processes, which reduced unit adsorption capacity; the removal rate was in positive correlation to dosage because the increase of the dosage provided more adsorption sites.[38] It is clear from this figure that ZrBC adsorptive effect was significantly more favorable than BC. Adsorption capacity was intersected with removal rate when a dosage was 0.125 $g \cdot L^{-1}$ for BC and 0.080 $g \cdot L^{-1}$ for ZrBC. Ensuring that the two materials were directly compared in same conditions, 0.125 $g \cdot L^{-1}$ (i.e., adsorbent mass of 0.010 g) was chosen for subsequent experiments. In this case, the adsorption capacity and removal rate of Sb(V) by ZrBC were 7.62 $mg \cdot g^{-1}$ and 99.07%, respectively. Accordingly, the optimum adsorbent dosage was identified as 0.125 $g \cdot L^{-1}$ and subsequent research was carried out under this condition.

2.2.2. Impact of Contact Time and Initial Sb(V) Concentration. Contact time is one of the important factors, and the result of its influence on Sb(V) adsorption is shown in Figure S3b. As shown in figure, adsorption capacities of BC

https://doi.org/10.1021/acsomega.5c01523
ACS Omega XXXX, XXX, XXX−XXX

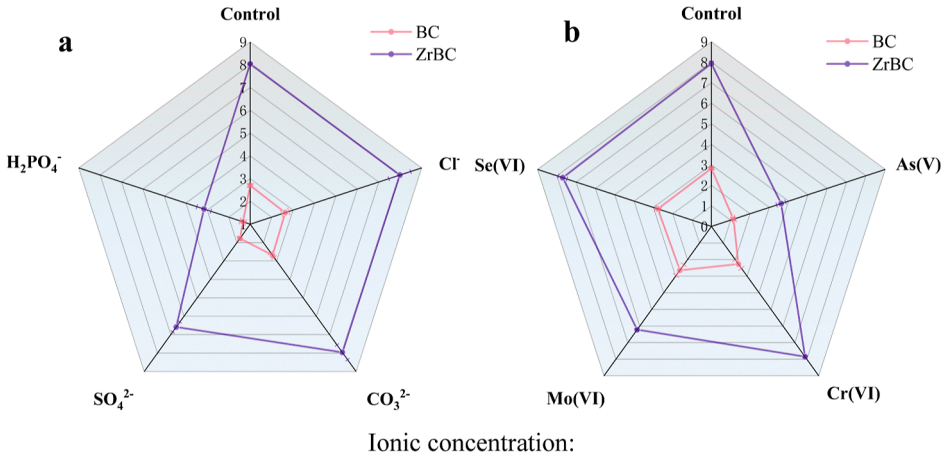

Figure 3. Impact from coexisting ions on Sb(V) adsorption by adsorbents. (a) Impact of coexisting anions. (b) Impact of coexisting metal ions.

and ZrBC rose rapidly within 30 min, reaching 3.33 and 7.96 mg·g^{-1}, respectively. This occurred because adsorbent provided abundant adsorptive sites during the initial reaction phase. After that, adsorption capacity was slowly increasing as time went by, finally reaching adsorption equilibrium within 360−720 min.

The relationship between initial Sb(V) concentration and adsorption capacity is presented in Figure S3c. As evidenced by this figure, the adsorption of ZrBC was always higher than BC. Sb(V) adsorption by BC and ZrBC increased promptly as preliminary concentration was raised from 0.2 to 3 mg·L^{-1}. Adsorption capacity raised slowly after preliminary concentration exceeded 3 mg·L^{-1}. This resulted from increasing initial concentration, which would increase chances for effective contact with adsorbent, allowing for increased adsorption capacity.[39] Additionally, the high concentration of Sb ions reduced the mass transfer resistance between the liquid and solid phases, which may be another factor contributing to the increase in adsorption capacity.[40]

2.2.3. Impact by Initial pH on Adsorption. Results for pH on adsorption by BC and ZrBC are shown in Figure S3e. Overall, Sb(V) adsorption of BC was low. Adsorptive result by ZrBC was better under acidic conditions, with the most significant results in the pH 2.0−4.0 range. As pH increased, the adsorptive effect tended to decrease. The greatest adsorptive effect was achieved with pH 3.0, with the adsorption capacity of ZrBC on Sb(V) of 8.57 mg·g^{-1}, and remaining concentration in the solution was less than 0.3 mg·L^{-1}, so pH remained at 3.0 for later experiments. The zeta potential is shown in Figure S3f. In the acidic environment, ZrBC surfaces were positively charged, especially when pH was less than 4.5, but negatively charged as pH increased.

$Sb(OH)_5$ was major form for Sb(V) at pH < 3.0; and when solution pH was 3.0−10.0, it was mainly present as $[Sb(OH)_6]^-$ (Figure S3d). Also, when pH 3.0−4.0, a large amount of H^+ increases the positive charge at adsorbent surfaces, resulting in high adsorption capacity of Sb(V). As pH increased, OH^- in solution grew, and $[Sb(OH)_6]^-$ had weaker adsorption affinity than OH^-, not conducive to adsorption.[41] The adsorption capacity increased when pH = 8.0 was probably because the surface charge, although negative, increased at this time. As liquid mixture pH was less than zero-point charge of ZrBC (pH_{zpc} = 4.50), the adsorbent surface protonated, increasing electrostatic attraction with $[Sb(OH)_6]^-$, which favored the adsorptive process. At higher pH, the deprotonation was enhanced, and electrostatic repulsion increased, and this can result in a reduced adsorptive effect.[42] This was approximately the same as the measurements of material zeta potential (Figure S3f). It was hypothesized that there were other mechanisms by which ZrBC adsorbed Sb(V) because adsorption capacities were still large when pH values were 2.0 and 5.0.

Above findings indicated adsorptive performance of ZrBC for Sb(V) was optimal when pH = 3.0.

2.2.4. Impact on Sb(V) Adsorption by Interfering Ions. More universal anions (CO_3^{2-}, SO_4^{2-}, Cl^-, $H_2PO_4^-$) were added to the solution to mimic the Sb(V) removal in practical water, which is possible to provide theoretical references for treating antimony-containing wastewater. Figure 3a shows what several anions do. For BC and ZrBC, the effect of adding CO_3^{2-} and Cl^- to the Sb(V) was marginal. The adsorption capacity of ZrBC was always greater as compared to BC. This was because Cl^- and CO_3^{2-} primarily complexed into outer spheres with the BC.,[43] hence having less effect on Sb(V) adsorption. The same observation was reached from Cumbal and SenGupta.[44] Influence of SO_4^{2-} and $H_2PO_4^-$ on Sb(V) adsorption was negative, both BC and ZrBC. SO_4^{2-} had relatively little influence compared to $H_2PO_4^-$, which was reduced by 34.39% and 18.09% for BC and ZrBC, respectively. The decrease in Sb(V) adsorption results from the relatively high affinity for SO_4^{2-} to adsorptive sites of the ZrBC surface.[45] When $H_2PO_4^-$ was added, Sb(V) adsorption was reduced by 50.42% and 60.72% for BC and ZrBC, respectively. Both phosphate and antimony are located in group 15 (VA group) of Periodic Table of Elements, thus having similar chemical structures.[46] Therefore, the presence of $H_2PO_4^-$ would severely hinder Sb(V) adsorption by BC and ZrBC.

Similar metal ions were added to the solution, which was essential to examine ZrBC adsorption selectivity on Sb(V). Arsenic(V), chromium(VI), molybdenum(VI) and selenium(VI) were selected for the research, and the effects are shown in Figure 3b. From the figure, it was clear that As(V) and Mo(VI) inhibited Sb(V) adsorption. Cr(VI) and Se(VI) showed little inhibition, and ZrBC reduced the adsorption capacity of Sb(V) by 1.13% and 3.02%, respectively. The addition of As(V) had the most obvious inhibitory effect,

https://doi.org/10.1021/acsomega.5c01523
ACS Omega XXXX, XXX, XXX−XXX

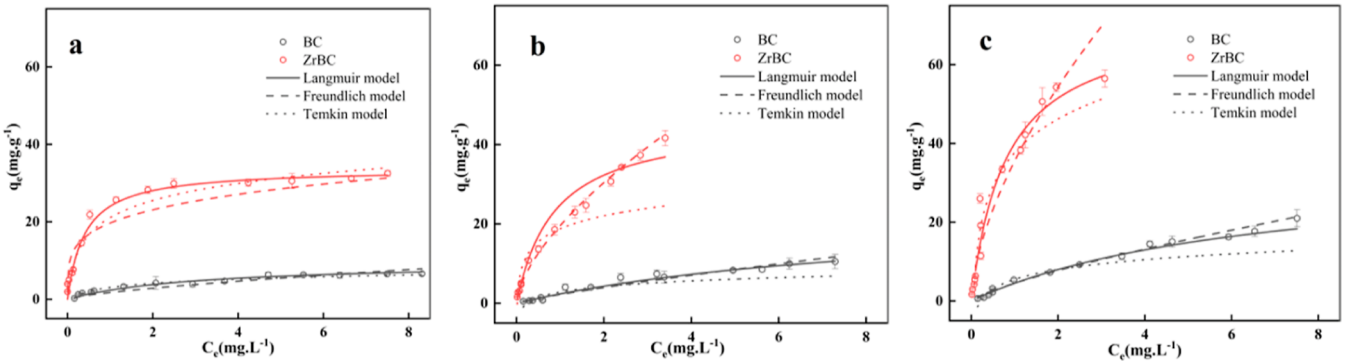

Figure 4. Adsorption isotherms for BC and ZrBC. (a) 25 °C. (b) 35 °C. (c) 45 °C.

Table 2. Isothermal Adsorption Fitting Parameters of Sb(V)

	Langmuir model			Freundlich model			Temkin model		
adsorption material	q_m (mg·g^{-1})	K_L (L·g^{-1})	R_L^2	K_F (L·g^{-1})	$1/n$	R_F^2	A (L·g^{-1})	K_T	R_T^2
25 °C BC	9.69	0.31	0.89	1.74	0.71	0.81	7.21	1608.81	0.99
25 °C ZrBC	33.75	2.46	0.71	19.69	0.23	0.90	27.37	388.94	0.97
35 °C BC	23.56	0.11	0.96	2.21	0.83	0.95	4.07	1273.98	0.79
35 °CZrBC	46.25	1.15	0.98	19.57	0.63	0.99	54.80	545.99	0.72
45 °C BC	34.62	0.14	0.97	4.53	0.76	0.97	4.60	734.40	0.92
45 °C ZrBC	72.34	1.23	0.94	35.56	0.61	0.90	21.13	214.25	0.95

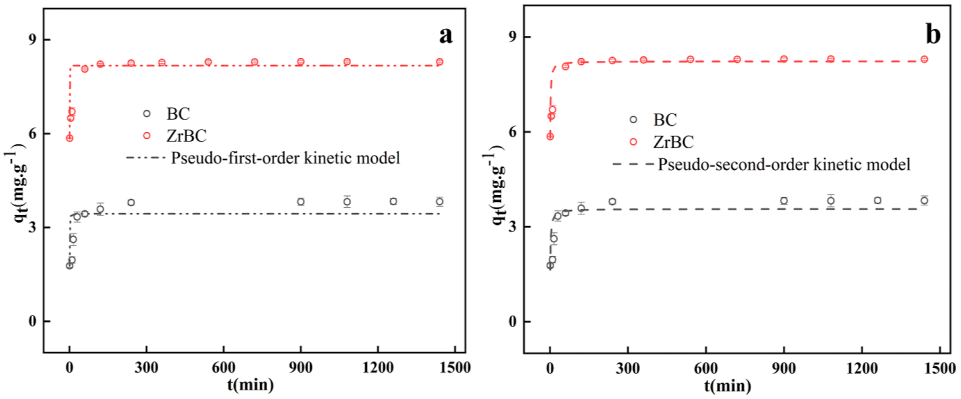

Figure 5. Adsorptive kinetics by BC and ZrBC. (a) PFO kinetic model. (b) PSO kinetic model.

decreasing Sb(V) adsorption 59.57% and 54.47% by BC and ZrBC, respectively. This resulted from that As(V) and Sb(V) had extremely similar chemical structures and easily competed with Sb(V) for the same adsorption site. Mo(VI) addition decreased Sb(V) adsorption capacity of ZrBC by 21.68%. It was ascribed to that Mo(VI) would form inner-sphere complexes with the adsorbent,[47] thus inhibiting the adsorption. Overall, ZrBC had some selective adsorption of Sb(V).

2.3. Isotherm Modeling. Used for assessing the adsorption capacity and interaction mechanisms of adsorbents, adsorption isotherms are important indicators for research on materials adsorption characterization. Data for Sb(V) was modeled by fitting Langmuir, Freundlich, and Temkin models. Figure 4 illustrates Langmuir, Freundlich, and Temkin models at three type temperatures (25, 35, and 45 °C), with relevant parameters listed in Table 2. Compared correlation coefficients R^2 at three temperatures indicated that BC fitted Langmuir modeling better, demonstrating adsorptive process was predominantly monolayer, and ZrBC had t highest fitting with Freundlich modeling, showing it was mainly a multilayer adsorption.[48]

According to Langmuir model, maximum adsorption capacity (q_m) by BC and ZrBC were at 45 °C, which were 34.62 and 72.34 mg·g^{-1}, respectively, and q_m of ZrBC was significantly higher than BC. R' values indicated that the adsorption properties were unfavorable ($R' > 1$), linear ($R' = 1$), favorable ($0 < R' < 1$), or irreversible ($R' = 0$).[49] According to Table 2 and eq S2, R' for both BC and ZrBC were less than 1 in three temperatures, suggesting good adsorptive processes. $1/n$ of Freundlich model indicated the exchange strength or surface nonuniformity. When $0 < 1/n < 1$, adsorptive processes was effective. The $1/n$ values were 0.23−0.63 L·g^{-1} for ZrBC on Sb(V) and 0.71−0.83 L·g^{-1} for BC at three different temperatures. $1/n$ were all lower than 1 indicating that adsorption occurred easily.[50] Temkin model was utilized to elucidate whether adsorption process involved electrostatic interactions.[51] Temkin model was well fitted as can be seen in Figure 4, suggesting electrostatic binding was one of the mechanism for BC and ZrBC adsorption, which was consistent with the analyses in pH effects.

2.4. Thermodynamic Analyzes of Sb(V) Adsorption by ZrBC. Ambient temperature is major element influencing

https://doi.org/10.1021/acsomega.5c01523
ACS Omega XXXX, XXX, XXX−XXX

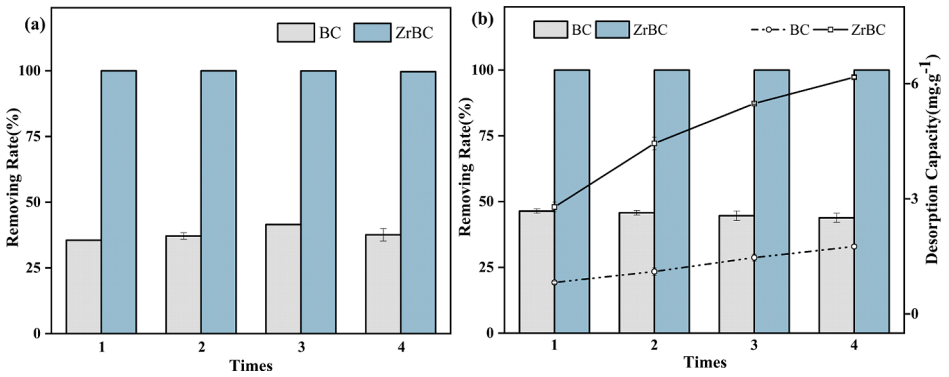

Figure 6. Reusability and reproducibility of BC and ZrBC. (a) Reusability. (b) Adsorption−desorption.

adsorptive procedures. Thus, the use of temperature as an analytical parameter in thermodynamic experiments is of paramount importance. The analysis findings are presented on Figure S4 with related data in Table S4. ΔG of each adsorbent at various temperatures was negative, showing that adsorptive process was feasible and spontaneous.[52] The Langmuir model showed that q_m of ZrBC was 33.75, 46.25, and 72.34 mg·g^{-1} at 25, 35, and 45 °C, respectively, which increased clearly as temperature rose (Table 2). Therefore, high temperature favored Sb(V) adsorption of ZrBC. The positive ΔH (39.98 kJ·mol^{-1}) of ZrBC indicated that it was an endothermic process and it preferred the adsorption with rising temperature, explaining q_m of ZrBC growth as temperature rose. Therefore, Sb(V) adsorption of ZrBC was a spontaneous endothermic process.

2.5. Adsorptive Kinetics of Adsorbent. Adsorptive kinetics can comprehensively understand the effect of adsorbent materials toward Sb(V) adsorptive process and is crucial for assessing adsorption behavior on materials. The pseudo-first-order (PFO) kinetic model and pseudo-second-order (PSO) kinetic model were utilized for matching the data. Figure 5a,b presents Sb(V) fitted curves, and Table S5 presents obtained parameters.

Two kinetic models were fitted with k values of 0.72 and 0.23 for BC and 1.25 and 0.29 for ZrBC, k values of ZrBC were all higher than BC, indicating that ZrBC had a faster adsorption speed for Sb(V).[42] This indicated that Zr modification added to the reactive sites fraction at adsorbent surface or possibly enhanced hole structure, leading to enhanced adsorption of Sb(V). This is consistent with the results of BET analysis. Their fitted q_e were all near the actual measurements. Both BC and ZrBC were more compatible with the proposed PSO (R^2 were 0.80 and 0.96), suggesting their Sb(V) adsorption were mainly chemisorption. Liu et al. reached analogous results.[39]

2.6. Reusability and Reproducibility of BC and ZrBC. Reusability and reproducibility of adsorbents are two important factors in determining their use. Figure 6 presents results on reusability and adsorption−desorption process of BC and ZrBC for Sb(V) adsorption. Overall adsorptive efficiency by BC was low as seen in the figure, with a slight increase in the removal rate after four repetitions. ZrBC adsorption capacity was almost unaffected as the repetition number increased. Sb(V) adsorption by ZrBC had potential for reusability.

NaOH was used as the desorbent. The experimental determinations indicated BC adsorptive capacity on Sb(V) tended to decrease with the rise of adsorption−desorption cycle times, whereas ZrBC adsorptive capacity was almost unaffected. Meanwhile, during the desorption process, concentration of Sb(V) desorbed gradually rose. Post four cycles, removal rate of BC decreased from 46.39% to 43.82%, and the desorption amount was 1.75 mg·g^{-1}; the removing rate of ZrBC could still be 100%, and the desorption amount was 6.16 mg·g^{-1}. The desorption of Sb can be attributed to NaOH leading to the excessive OH^- in the solution, and Sb was desorbed by combining with this portion of OH^-. The decrease in the adsorption of Sb may result from losing active sites on material surface and impregnated particles.[53] In summary, in terms of recycling, ZrBC performed better than BC and has the potential to reduce Sb in water.

Therefore, adsorptive ability of ZrBC was better than that of BC. Sb(V) could be successfully desorbed from ZrBC that showed reusable potential even after multiple application cycles, increasing its value for Sb(V) treatment applications in water.

2.7. Application of ZrBC in Real Wastewaters. Figure 7 demonstrates effects of ZrBC dosage for Sb removing in actual

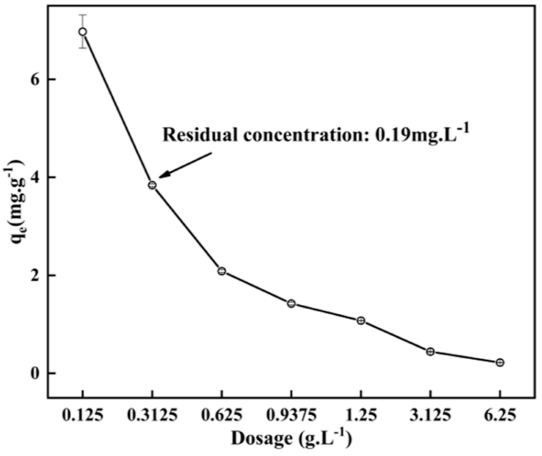

Figure 7. Effect of ZrBC dosage on actual wastewater.

antimony mine wastewater (Sb concentration was 1.37 mg·L^{-1}.). As ZrBC dosage increased, Sb concentration of wastewater tended to decrease significantly. ZrBC q_e for real water was lower than that of simulated wastewater. When ZrBC dosage as 0.125 g·L^{-1}, q_e was 6.97 mg·g^{-1}. It was due the complication with background compositions in practical wastewater and existence of numerous substances (such as and SO_4^{2-}) (Table S6) which probably compete against Sb.

https://doi.org/10.1021/acsomega.5c01523
ACS Omega XXXX, XXX, XXX−XXX

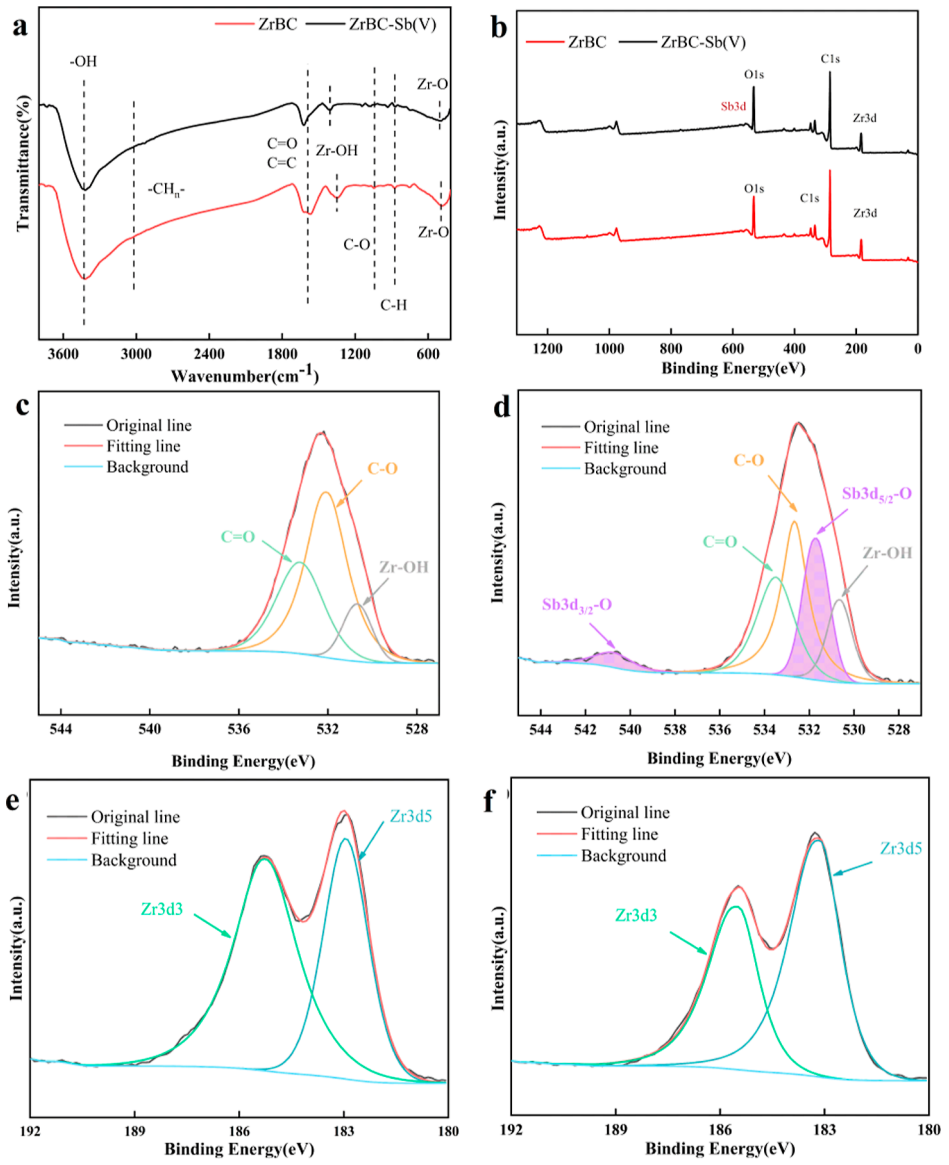

Figure 8. FT-IR and XPS spectra of ZrBC before and after Sb(V) adsorption. (a) FT-IR. (b) XPS, full spectra. (c), (d) XPS, O 1s spectra. (e), (f) XPS, Zr 3d spectra.

When ZrBC increasing further toward 0.3125 g·L^{-1}, the residual Sb concentration in water was 0.19 mg·L^{-1}, below 0.3 mg·L^{-1} emission limit (GB 30770-2014). In summary, ZrBC had potential for practical applications.

2.8. Mechanism of ZrBC Adsorption of Sb(V) in Water. Adsorptive experiments show ZrBC has better adsorption effect on Sb(V) compared with BC. To further investigate the removal mechanism, ZrBC before and after Sb(V) adsorption were characterized using BET, FT-IR, and XPS.

Surface properties before and after adsorption were investigated by BET analysis. Related parameters are listed in Table S3. After Sb(V) adsorption, the specific surface area and total pore volume of BC and ZrBC decreased 46.66 m^3·g^{-1} and 0.028 cm^3·g^{-1}, respectively, showing the function of pore filling for Sb(V) adsorption.[54]

FT-IR spectroscopy can analyze surface functional groups of ZrBC, as well as variations subsequent to Sb(V) adsorption. The FT-IR before and after adsorption of Sb(V) is shown in Figure 8a. ZrBC adsorption for Sb(V) resulted in a drop on −OH peak. This was because hydroxyl group could serve as a hydrogen donor and formed hydrogen bonds with the oxygen atoms on Sb(V).[54] Sb(V) adsorption by ZrBC showed a shifted at Zr−OH peak, due to ligand exchange of Zr−OH with Sb. Absorption peak at 493 cm^{-1} was reduced after Sb(V) adsorption, by forming inner-sphere Zr−O−Sb complexes through empty d-orbitals of Zr.

Sb 3d existence proved satisfactory Sb adsorption by ZrBC (Figure 8b,d). The O 1s spectra of BC before and after Sb(V) adsorption are given in Figure 8c,d. After adsorption, Sb $3d_{5/2}$-O and Sb $3d_{3/2}$-O peaks appeared, indicating successful Sb adsorption on ZrBC. Sb $3d_{5/2}$-O and Sb $3d_{3/2}$-O were at 531.69 and 540.74 eV, respectively, representing Sb(V).[55] Table S7 shows that after Sb(V) adsorption, the C═O content decreased from 32.36% to 24.59%, and C−O reduced from 55.41% to 33.67%. This may be due to their complex formation with Sb(V). Zr 3d spectra of ZrBC were all characterized by two peaks (Figure 8e,f), belonging to the Zr 3d5 and Zr 3d3 electronic orbitals.[15] Adsorption of Sb(V) by ZrBC increased the binding energy of the Zr 3d peak by about

https://doi.org/10.1021/acsomega.5c01523
ACS Omega XXXX, XXX, XXX−XXX

0. Twenty-three and 0.25 eV, respectively, which was due to the binding between Sb and Zr. Zirconium faced a large electron abstraction when bonded to it and tended to lose electron density, resulting increased bonding energies of Zr 3d5 and Zr 3d3.[56] In addition, Zr−OH may undergo ligand exchange with Sb.[57]

According to aforementioned results, Figure 9 describes the adsorptive mechanism diagram of ZrBC on Sb(V) in water, including pore filling, ligand exchange, complexation, hydrogen bonding, and electrostatic interactions.

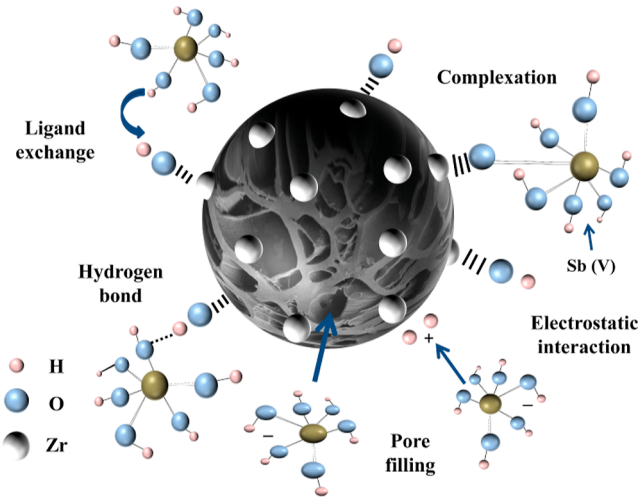

Figure 9. Diagram of the mechanism of Sb(V) adsorption by ZrBC.

3. CONCLUSIONS

3.1. Shortcomings and Future Prospects. Research found ZrBC efficiently removes trace Sb(V) and shows strong environmental adaptability. Despite these promising findings, certain limitations remain. To advance the practical application of ZrBC, future research should focus on the following two aspects: (1) accounting for the complex environmental conditions of natural waters and further enhancing adsorptive property, and (2) evaluating ZrBC adsorptive ability under dynamic flow conditions to better simulate real-world scenarios.

3.2. Conclusions. In this study, peanut shells, an agricultural waste, were modified to obtain a novel zirconium-modified BC (ZrBC) for the treatment of Sb(V) wastewater. The results showed that ZrBC could effectively remove low concentrations of Sb(V) from water and achieved resourceful use of peanut shell solid waste. ZrBC had ability to adsorb Sb(V) from water with the q_m of 72.34 mg·g^{-1} at pH 3.0, contact time of 720 min, and dosage of 0.125 g·L^{-1}. For most of the coexisting ions (Cr(VI), Se(VI), Mo(VI), CO_3^{2-}, SO_4^{2-}, Cl^-), the ZrBC adsorption was not strongly affected by them, and the inhibition effect ranged from 0.74% to 21.68%. Isothermal (Freundlich model, R^2 = 0.90−0.99) analyses indicated that Sb(V) adsorption on ZrBC was a multilayer, and kinetic (PSO kinetic model, R^2 = 0.96) revealed that the adsorption process was mainly chemisorption. Thermodynamic research indicated that the adsorption process was heat-absorbing and spontaneous. After four repetitions and adsorption−desorption, the Sb(V) removal rate was stable at 100%, and q_e of ZrBC for Sb in actual wastewater was 6.97 mg·g^{-1} at 0.125 g·L^{-1} dosage. These experimental results showed that the ZrBC had some practical application value. Pore filling, ligand exchange, complexation, hydrogen bonding, and electrostatic interactions dominate the immobilization of Sb(V) in the aqueous environment. In conclusion, ZrBC significantly enhanced the adsorption capacity and it is an effective adsorption material, which can provide theoretical information and practical basis for the field of Sb adsorption.

4. MATERIALS AND METHODS

4.1. Materials and Instruments. Peanut shells were produced in Nanyang, Henan Province. Tables S1 and S2 list the chemistries and instrumentation information needed to accomplish experiments.

4.2. Prepare for BC. *4.2.1. Preparation of Original BC.* Peanut shells were removed from impurities, desiccated at 90 °C over 12 h, then powdered. The powder was placed in a tube furnace and then heated to 550 °C at a heating rate of 7 °C·min^{-1} in a stable N_2 environment (2 h) to obtain peanut shell BC. The solid product was moved, washed to remove the ash, desiccated at 80 °C, milled, and sifted with a 100 mesh filter. The resulting BC was marked as BC.

4.2.2. Prepare for Zirconium-Modified BC. The coprecipitation method was used to synthesize zirconium-modified BC. BC was added to 1% $ZrOCl_2·8H_2O$ solution (the mass ratio of BC and $ZrOCl_2·8H_2O$ was kept at 1:1) and mixed well by magnetic stirring. pH was adjusted as high as 10 using 10% NaOH and stirred continuously for 1 h. The supernatant was then filtered through a glass loophole. The precipitate was cleaned and dried at 80 °C. Zirconium-modified biochar (ZrBC) was obtained, dried, and stored away from light for later use.

4.3. Adsorption Experiments of Sb(V) by BC and ZrBC. Adsorptive performance of BC and ZrBC for Sb(V) was analyzed by batch adsorption tests under different environmental factors, i.e., dose, contact time, initial Sb(V) concentration, solution pH, and interfering ions. Different doses (0.0625, 0.1, 0.125, 0.25, 0.625, 1, and 1.25 g·L^{-1}), contact times (1, 5, 10, 15, 30, 60, 120, 240, 360, 540, 720, 900, 1,080, 1,260, and 1440 min), initial Sb(V) concentration (0.2, 0.4, 0.6, 0.8, 1, 2, 3, 4, 5, 6, 7, 8, 9, and 10 mg·L^{-1}), and pH (2.0, 3.0, 4.0, 5.0, 6.0, 7.0, 8.0, 9.0, and 10.0) were investigated. In order to assess adsorptive property of ZrBC for Sb(V) in a complex ionic environment, several ions were selected as the interfering ions, including the anions CO_3^{2-}, $H_2PO_4^-$, SO_4^{2-}, and Cl^-, with the concentration set at 1 mmol·L^{-1}; and the metal ions similar to Sb, arsenic(V), chromium(VI), molybdenum(VI) and selenium(VI), with the concentration set to 0.1 mmol·L^{-1}. In isotherm tests, Sb(V) at concentrations of 0.2−10 mg·L^{-1} was shaken for 720 min in 25 °C. Similarly, experiments were conducted at 35 and 45 °C for thermodynamic analyses. In kinetic experiments, samples were collected at different times (1−1440 min) from Sb(V) solutions. In the repeatability experiments, four adsorption reactions were repeated with the adsorbent. In the cyclic regeneration test, four adsorption−desorption runs were performed with a 1% NaOH solution as the desorbent. Actual antimony-containing wastewater from the mine was taken to study the effectiveness of ZrBC in the real environment.

All samples were filtered through 0.45 μm membranes, and Sb(V) concentrations were determined by hydride generation dual-channel atomic fluorescence spectrometry (HG-AFS). 1 mL of the supernatant filtrate after the reaction was taken in a 10 mL centrifuge tube, 1 mL of 50% HCl and 1 mL of 5%

https://doi.org/10.1021/acsomega.5c01523
ACS Omega XXXX, XXX, XXX−XXX

thiourea−ascorbic acid solution were added. The volume was fixed to 10 mL and then determined the antimony concentration in the solution after a full reaction for 30 min in a thermostat at 30 °C. All adsorption experiments were performed in triplicate, and data were expressed as mean ± standard deviation (n = 3).

4.4. Characterization of Materials. Materials were characterized by SEM and EDS, including both pre and post modification and adsorption. The pore volume, specific surface area, and pore size of the BC were calculated via a BET analyzer. The differences in surface functional groups of BC and ZrBC before and after adsorption of Sb(V) were investigated by FT-IR. XRD was used to probe adsorbent crystal structure, and the valence changes of the relevant elements on the surface of the adsorbents were determined by XPS for adsorbents. The zeta potentials of material surfaces under different pH values were determined by the zeta-potential analyzer.

4.5. Data Processing. The formula for adsorption is given in eq S1. Langmuir, Freundlich, and Temkin models were utilized for fitting isothermal adsorptive data. Appropriate equations are eqs S2−S4. In the adsorption thermodynamic experiments, an equation of Van't-Hoff was utilized for the calculation of thermodynamic parameters. The calculation equation is shown in eq S5. The data on the adsorption kinetics experiments were simulated using PFO and PSO kinetic models, and eqs S6 and S7 are the corresponding equations.

■ ASSOCIATED CONTENT

Supporting Information

The Supporting Information is available free of charge at https://pubs.acs.org/doi/10.1021/acsomega.5c01523.

Formulas, EDS and BET images, XPS full spectra of BC and ZrBC XPS full spectra of BC and ZrBC, thermodynamic functions of ZrBC, chemicals relevant information, instruments description, BC and ZrBC surface properties, thermodynamic parameters of Sb(V) adsorbed, kinetic parameters for the adsorption of Sb(V), test results of mines wastewater, and relative content of elements in each material (PDF)

■ AUTHOR INFORMATION

Corresponding Author

Siqin Xu − *Key Laboratory of Karst Georesources and Environment, Ministry of Education, Guizhou University, Guiyang, Guizhou 550025, China; College of Resources and Environmental Engineering, Guizhou University, Guiyang, Guizhou 550025, China;* orcid.org/0009-0000-7555-5201; Phone: +86 13639085421; Email: sqxu1@gzu.edu.cn

Authors

Xueyi Shen − *Key Laboratory of Karst Georesources and Environment, Ministry of Education, Guizhou University, Guiyang, Guizhou 550025, China; College of Resources and Environmental Engineering, Guizhou University, Guiyang, Guizhou 550025, China*

Siyi Ma − *Key Laboratory of Karst Georesources and Environment, Ministry of Education, Guizhou University, Guiyang, Guizhou 550025, China; College of Resources and Environmental Engineering, Guizhou University, Guiyang, Guizhou 550025, China*

Complete contact information is available at: https://pubs.acs.org/10.1021/acsomega.5c01523

Author Contributions

All authors contributed to the study conception and design. Material preparation, data collection, and analysis were performed by Xueyi Shen and Siyi Ma. The first draft of the manuscript was written by [Xueyi Shen], and all authors commented on previous versions of the manuscript. All authors read and approved the final manuscript.

Notes

Ethical Approval (Compliance with Ethical Standards) (Consent to Participate) All authors whose names appear on the submission made substantial contributions to the conception or design of the work. All authors signed their names to the manuscript approved the version to be published. The authors declare no competing financial interest.

■ ACKNOWLEDGMENTS

This work was supported by the National Natural Science Foundation of China (41062007). The authors thank Shiyanjia Lab (http://www.shiyanjia.com) for providing characterization instruments.

■ REFERENCES

(1) Tang, H.; Hassan, M. U.; Nawaz, M.; Yang, W.; Liu, Y.; Yang, B. A review on sources of soil antimony pollution and recent progress on remediation of antimony polluted soils. *Ecotoxicol. Environ. Saf.* **2023**, *266*, 115583.

(2) Bolan, N.; Kumar, M.; Singh, E.; Kumar, A.; Singh, L.; Kumar, S.; Keerthanan, S.; Hoang, S. A.; El-Naggar, A.; et al. Antimony contamination and its risk management in complex environmental settings: A review. *Environ. Int.* **2022**, *158*, 106908.

(3) Xu, R.; Sun, X.; Han, F.; Li, B.; Xiao, E.; Xiao, T.; Yang, Z.; Sun, W. Impacts of antimony and arsenic co-contamination on the river sedimentary microbial community in an antimony-contaminated river. *Sci. Total Environ.* **2020**, *713*, 136451.

(4) Lu, H.; Zhang, W.; Tao, L.; Liu, F.; Zhang, J. Enhanced removal of antimony by acid birnessite with doped iron ions: Companied by the structural transformation. *Chemosphere* **2019**, *226*, 834−840.

(5) Tu, Y.; Wang, S.; Lu, Y.; Chan, T.; Johnston, C. T. New insight in adsorption of Sb(III)/Sb(V) from waters using magnetic nanoferrites: X-ray absorption spectroscopy investigation. *J. Mol. Liq.* **2021**, *330*, 115691.

(6) Yan, M.; Xi, Y.; Jiang, N.; Li, Q.; Zheng, S.; Hu, Y.; Liu, Y.; Bao, W.; Huang, M. High-performance thin film composite forward osmosis membrane for efficient rejection of antimony and phenol from wastewater: Characterization, performance, and MD-DFT simulation. *J. Membr. Sci.* **2024**, *703*, 122847.

(7) Guo, W.; Fu, Z.; Wang, H.; Liu, S.; Wu, F.; Giesy, J. P. Removal of antimonate (Sb(V)) and antimonite (Sb(III)) from aqueous solutions by coagulation-flocculation-sedimentation (CFS): Dependence on influencing factors and insights into removal mechanisms. *Sci. Total Environ.* **2018**, *644*, 1277−1285.

(8) Oehmen, A.; Viegas, R.; Velizarov, S.; Reis, M. A. M.; Crespo, J. G. Removal of heavy metals from drinking water supplies through the ion exchange membrane bioreactor. *Desalination* **2006**, *199*, 405−407.

(9) Xu, R.; Li, Q.; Nan, X.; Yang, Y.; Xu, B.; Li, K.; Wang, L.; Zhang, Y.; Jiang, T. Synthesis of nano-silica and biogenic iron (oxyhydr) oxides composites mediated by iron oxidizing bacteria to remove antimonite and antimonate from aqueous solution: Performance and mechanisms. *J. Hazard. Mater.* **2022**, *422*, 126821.

(10) Song, P.; Yang, Z.; Zeng, G.; Yang, X.; Xu, H.; Huang, J.; Wang, L. Optimization, kinetics, isotherms, and thermodynamics studies of

antimony removal in electrocoagulation process. *Water, Air, Soil Pollut.* **2015**, *226*, 380.
(11) Yang, X.; Zhou, B.; Wang, C.; Tan, R.; Cheng, S.; Saleem, A.; Zhang, Y. Mesoporous silica nanoparticles for the uptake of toxic antimony from aqueous matrices. *ACS Omega* **2023**, *8*, 26916−26925.
(12) Peng, L.; Wang, N.; Xiao, T.; Wang, J.; Quan, H.; Fu, C.; Kong, Q.; Zhang, X. A critical review on adsorptive removal of antimony from waters: Adsorbent species, interface behavior and interaction mechanism. *Chemosphere* **2023**, *327*, 138529.
(13) Hu, Y.; Guo, T.; Xia, F.; Wang, Z.; Wang, W.; Wang, Y.; Ma, S. Phosphorus-zirconium co-doped walnut shell biochar prepared by pyrolysis for efficient Pb (II) captured from synthetic wastewater. *J. Environ. Chem. Eng.* **2023**, *11*, 110964.
(14) Li, J.; Li, X.; Hayat, T.; Alsaedi, A.; Chen, C. Screening of zirconium-based metal-organic frameworks for efficient simultaneous removal of antimonite (Sb(III)) and antimonate (Sb(V)) from aqueous solution. *ACS Sustain. Chem. Eng.* **2017**, *5*, 11496−11503.
(15) Yu, Z.; Xu, C.; Yuan, K.; Gan, X.; Feng, C.; Wang, X.; Zhu, L.; Zhang, G.; Xu, D. Characterization and adsorption mechanism of ZrO_2 mesoporous fibers for health-hazardous fluoride removal. *J. Hazard. Mater.* **2018**, *346*, 82−92.
(16) Tang, Y.; Liu, D.; He, H.; Zou, J.; Wang, D.; Yang, X.; Zhang, L.; Yang, C. Immobilization of zirconium-modified activated carbon in an alginate matrix for the removal of atrazine: Preparation, performances and mechanisms. *Environ. Technol. Innov.* **2024**, *35*, 103699.
(17) Zhou, J.; Liu, Y.; Li, B.; Huang, W.; Qin, J.; Li, H.; Chen, G. Hydrous zirconium oxide modified biochar for in situ remediation of arsenic contaminated agricultural soil. *J. Environ. Chem. Eng.* **2022**, *10*, 108360.
(18) Ao, H.; Cao, W.; Hong, Y.; Wu, J.; Wei, L. Adsorption of sulfate ion from water by zirconium oxide-modified biochar derived from pomelo peel. *Sci. Total Environ.* **2020**, *708*, 135092.
(19) Xie, Y.; Wang, L.; Li, H.; Westholm, L. J.; Carvalho, L.; Thorin, E.; Yu, Z.; Yu, X.; Skreiberg, Ø. A critical review on production, modification and utilization of biochar. *J. Anal. Appl. Pyrolysis* **2022**, *161*, 105405.
(20) Patra, B. R.; Mukherjee, A.; Nanda, S.; Dalai, A. K. Biochar production, activation and adsorptive applications: a review. *Environ. Chem. Lett.* **2021**, *19*, 2237−2259.
(21) Yang, X.; Tian, X.; Xue, Y.; Wang, C. Application of iron-modified biochar in the fields of adsorption and degradation of antibiotics. *J. Environ. Manage.* **2025**, *380*, 124875.
(22) Ji, J.; Xu, S.; Ma, Z.; Mou, Y. Optimisation of preparation conditions and removal mechanism for trivalent antimony by biochar-supported nano zero-valent iron. *Environ. Technol.* **2022**, *26*, 102240.
(23) Chon, K.; Mo Kim, Y.; Bae, S. Advances in Fe-modified lignocellulosic biochar: Impact of iron species and characteristics on wastewater treatment. *Bioresour. Technol.* **2024**, *395*, 130332.
(24) Ullah, I.; Baig, S. A.; Zaheer, H.; Shams, D. F.; Bibi, H.; Khan, W.; Xu, X.; Danish, M. Application of magnetically recoverable biochar amended zirconium adsorbent composite for enhanced As(III, V) removal from aqueous solutions. *Water, Air, Soil Pollut.* **2025**, *236*, 46.
(25) Peng, Y.; Azeem, M.; Li, R.; Xing, L.; Li, Y.; Zhang, Y.; Guo, Z.; Wang, Q.; Ngo, H. H.; et al. Zirconium hydroxide nanoparticle encapsulated magnetic biochar composite derived from rice residue: Application for As(III) and As(V) polluted water purification. *J. Hazard. Mater.* **2022**, *423*, 127081.
(26) Mei, L.; Qiao, H.; Ke, F.; Peng, C.; Hou, R.; Wan, X.; Cai, H. One-step synthesis of zirconium dioxide-biochar derived from Camellia oleifera seed shell with enhanced removal capacity for fluoride from water. *Appl. Surf. Sci.* **2020**, *509*, 144685.
(27) Banerjee, S.; Joshi, S. R.; Mandal, T.; Halder, G. Application of zirconium caged activated biochar alginate beads towards deionization of Cr(VI) laden water in a fixed bed column reactor. *J. Environ. Chem. Eng.* **2018**, *6*, 4018−4029.
(28) Zhang, W.; Mao, S.; Chen, H.; Huang, L.; Qiu, R. Pb(II) and Cr(VI) sorption by biochars pyrolyzed from the municipal wastewater sludge under different heating conditions. *Bioresour. Technol.* **2013**, *147*, 545−552.
(29) Huang, Q.; Luo, K.; Pi, Z.; He, L.; Yao, F.; Chen, S.; Hou, K.; Liu, Y.; Li, X.; Yang, Q. Zirconium-modified biochar as the efficient adsorbent for low-concentration phosphate: performance and mechanism. *Environ. Sci. Pollut. Res.* **2022**, *29*, 62347−62360.
(30) Park, S.; Lee, Y.; Kang, J.; Lee, J.; Lee, C. Application of Fe-impregnated biochar from cattle manure for removing pentavalent antimony from aqueous solution. *Appl. Sci.* **2021**, *11*, 9257.
(31) Chia, C. H.; Gong, B.; Joseph, S. D.; Marjo, C. E.; Munroe, P.; Rich, A. M. Imaging of mineral-enriched biochar by FTIR, Raman and SEM−EDX. *Vib. Spectrosc.* **2012**, *62*, 248−257.
(32) Perveen, S.; Nadeem, R.; Nosheen, F.; Asjad, M. I.; Awrejcewicz, J.; Anwar, T. Biochar-mediated zirconium ferrite nanocomposites for tartrazine dye removal from textile wastewater. *Nanomaterials* **2022**, *12*, 2828.
(33) Wu, Q.; Xian, Y.; He, Z.; Zhang, Q.; Wu, J.; Yang, G.; Zhang, X.; Qi, H.; Ma, J.; Xiao, Y.; et al. Adsorption characteristics of Pb(II) using biochar derived from spent mushroom substrate. *Sci. Rep.* **2019**, *9*, 15999.
(34) Sahu, N.; Singh, J.; Koduru, J. R. Removal of arsenic from aqueous solution by novel iron and iron-zirconium modified activated carbon derived from chemical carbonization of Tectona grandis sawdust: Isotherm, kinetic, thermodynamic and breakthrough curve modelling. *Environ. Res.* **2021**, *200*, 111431.
(35) Ayanwusi, O. R.; Abdulkareem, S. A.; Michael, T. T.; Iwuozor, K. O.; Emenike, E. C.; Hambali, H. U.; Adeniyi, A. G. Characterization of groundnut shell biochar produced with different stainless steel combustion compartment volumes. *Biofuel Bioprod. Biorefining* **2024**, *18*, 1598−1612.
(36) Hu, S.; Luo, H.; Li, C.; Yi, K.; Song, J.; Ji, C.; Yang, W. Selective recovery of high purity aluminium phosphate from incinerated sewage sludge ash with Zr-modified biochar. *J. Clean. Prod.* **2024**, *446*, 141463.
(37) Musyarofaha; Soontaranon, S.; Limphirat, W.; Triwikantoroa; Pratapa, S. XRD, WAXS, FTIR, and XANES studies of silica-zirconia systems. *Ceram. Int.* **2019**, *45*, 15660−15670.
(38) Aljerf, L. High-efficiency extraction of bromocresol purple dye and heavy metals as chromium from industrial effluent by adsorption onto a modified surface of zeolite: Kinetics and equilibrium study. *J. Environ. Manage.* **2018**, *225*, 120−132.
(39) Liu, C.; Li, Y.; Wang, X.; Li, B.; Zhou, Y.; Liu, D.; Liu, D.; Liu, S. Efficient extraction of antimony(III) by titanate nanosheets: Study on adsorption behavior and mechanism. *Ecotoxicol. Environ. Saf.* **2021**, *207*, 111271.
(40) Ahmad, I.; Farwa, U.; Khan, Z. U. H.; Imran, M.; Khalid, M. S.; Zhu, B.; Rasool, A.; Shah, G. M.; Tahir, M.; et al. Biosorption and health risk assessment of arsenic contaminated water through cotton stalk biochar. *Surf. Interfaces* **2022**, *29*, 101806.
(41) Jia, X.; Zhou, J.; Liu, J.; Liu, P.; Yu, L.; Wen, B.; Feng, Y. The antimony sorption and transport mechanisms in removal experiment by Mn-coated biochar. *Sci. Total Environ.* **2020**, *724*, 138158.
(42) Rahman, M. A.; Rahman, M. M.; Bahar, M.; Sanderson, P.; Lamb, D. Transformation of antimonate at the biochar-solution interface. *ACS ES&T Water* **2021**, *1*, 2029−2036.
(43) Rahman, M. A.; Rahman, M. M.; Bahar, M. M.; Sanderson, P.; Lamb, D. Antimonate sequestration from aqueous solution using zirconium, iron and zirconium-iron modified biochars. *Sci. Rep.* **2021**, *11*, 8113.
(44) Cumbal, L.; SenGupta, A. K. Arsenic removal using polymer-supported hydrated Iron(III) oxide nanoparticles: Role of donnan membrane effect. *Environ. Sci. Technol.* **2005**, *39*, 6508−6515.
(45) Zhang, L.; Dong, Y.; Liu, J.; Liu, C.; Liu, W.; Lin, H. The effect of co-pyrolysis temperature for iron-biochar composites on their adsorption behavior of antimonite and antimonate in aqueous solution. *Bioresour. Technol.* **2022**, *347*, 126362.
(46) Wang, L.; Wang, J.; Wang, Z.; He, C.; Lyu, W.; Yan, W.; Yang, L. Enhanced antimonate (Sb(V)) removal from aqueous solution by La-doped magnetic biochars. *Chem. Eng. J.* **2018**, *354*, 623−632.

https://doi.org/10.1021/acsomega.5c01523
ACS Omega XXXX, XXX, XXX−XXX

(47) Verbinnen, B.; Block, C.; Lievens, P.; Van Brecht, A.; Vandecasteele, C. Simultaneous removal of molybdenum, antimony and selenium oxyanions from wastewater by adsorption on supported magnetite. *Waste Biomass Valorization* **2013**, *4*, 635−645.
(48) Zhou, Y.; Liu, X.; Xiang, Y.; Wang, P.; Zhang, J.; Zhang, F.; Wei, J.; Luo, L.; Lei, M.; Tang, L. Modification of biochar derived from sawdust and its application in removal of tetracycline and copper from aqueous solution: Adsorption mechanism and modelling. *Bioresour. Technol.* **2017**, *245*, 266−273.
(49) Foo, K. Y.; Hameed, B. H. Insights into the modeling of adsorption isotherm systems. *Chem. Eng. J.* **2010**, *156*, 2−10.
(50) Bordoloi, N.; Goswami, R.; Kumar, M.; Kataki, R. Biosorption of Co(II) from aqueous solution using algal biochar: Kinetics and isotherm studies. *Bioresour. Technol.* **2017**, *244*, 1465−1469.
(51) Xu, R.; Li, Q.; Nan, X.; Yang, Y.; Xu, B.; Li, K.; Wang, L.; Zhang, Y.; Jiang, T. Synthesis of nano-silica and biogenic iron (oxyhydr) oxides composites mediated by iron oxidizing bacteria to remove antimonite and antimonate from aqueous solution: Performance and mechanisms. *J. Hazard. Mater.* **2022**, *422*, 126821.
(52) Ji, J.; Xu, S.; Ma, Z.; Mou, Y. Trivalent antimony removal using carbonaceous nanomaterial loaded with zero-valent bimetal (iron/copper) and their effect on seed growth. *Chemosphere* **2022**, *296*, 134047.
(53) Wang, X.; Zheng, M.; Qian, Y.; Chen, H.; Li, X.; Li, X.; Zhang, A.; Xue, G. Synergizing redox of zerovalent iron and singlet oxygen to remove aniline, chromium and antimony in printing and dyeing wastewater synchronously: Multifunctional effect of sludge derived biochar. *Chem. Eng. J.* **2023**, *476*, 146927.
(54) Chen, H.; Gao, Y.; El-Naggar, A.; Niazi, N. K.; Sun, C.; Shaheen, S. M.; Hou, D.; Yang, X.; Tang, Z.; et al. Enhanced sorption of trivalent antimony by chitosan-loaded biochar in aqueous solutions: Characterization, performance and mechanisms. *J. Hazard. Mater.* **2022**, *425*, 127971.
(55) Wu, T.; Sun, Q.; Fang, G.; Cui, P.; Liu, C.; Alves, M. E.; Qin, W.; Zhou, D.; Shi, Z.; Wang, Y. Unraveling the effects of gallic acid on Sb(III) adsorption and oxidation on goethite. *Chem. Eng. J.* **2019**, *369*, 414−421.
(56) Wang, X.; Pan, S.; Zhang, M.; Qi, J.; Sun, X.; Gu, C.; Wang, L.; Li, J. Modified hydrous zirconium oxide/PAN nanofibers for efficient defluoridation from groundwater. *Sci. Total Environ.* **2019**, *685*, 401−409.
(57) Guo, Y.; Zhang, X.; Xie, N.; Guo, R.; Wang, Y.; Sun, Z.; Li, H.; Jia, H.; Niu, D.; Sun, H. B. Investigation of antimony adsorption on a zirconium-porphyrin-based metal-organic framework. *Dalton Trans.* **2021**, *50*, 13932−13942.

https://doi.org/10.1021/acsomega.5c01523
ACS Omega XXXX, XXX, XXX−XXX